
Article:
Al-Tameemi, H.A., Long, H. orcid.org/0000-0003-1673-1193 and Dwyer-Joyce, R.S. (2019) Damage characterisation of white etching cracks in a black oxide coated wind turbine gearbox bearing. Wear, 432-433. 102923. ISSN 0043-1648

https://doi.org/10.1016/j.wear.2019.05.038

Accepted Manuscript

Damage characterisation of white etching cracks in a black oxide coated wind turbine gearbox bearing

H.A. Al-Tameemi, H. Long, R.S. Dwyer-Joyce

PII: S0043-1648(18)31406-6

DOI: https://doi.org/10.1016/j.wear.2019.05.038

Reference: WEA 102923

To appear in: *Wear*

Received Date: 8 November 2018

Revised Date: 16 May 2019

Accepted Date: 31 May 2019

Please cite this article as: H.A. Al-Tameemi, H. Long, R.S. Dwyer-Joyce, Damage characterisation of white etching cracks in a black oxide coated wind turbine gearbox bearing, *Wear* (2019), doi: https://doi.org/10.1016/j.wear.2019.05.038.

Damage characterisation of white etching cracks in a black oxide coated wind turbine gearbox bearing

H. A. Al-Tameemi, H. Long* and R. S. Dwyer-Joyce

Department of Mechanical Engineering, The University of Sheffield, Sheffield, UK.

*Corresponding author: Dr Hui Long (Email: h.long@sheffield.ac.uk, Tel: +44 (0) 114 222 7759)

Abstract

White Etching Cracks (WECs) have been reported to be the main cause of premature failure of Wind Turbine Gearbox (WTG) bearings however their failure mechanisms and damage initiators are still being investigated. An industrial solution of Black Oxide (BO) coating has been in use to prolong the life of the WTG bearings. This study reports an examination of microstructural damage observed on a failed BO coated WTG bearing. Variations of hardness and modulus of elasticity across the thickness of the BO coating layer were measured and showed the evidence of wear-out of this layer after WTG field operation. Microstructural damage observed in this bearing was similar to that found in uncoated WTG bearings. The findings provided new evidence showing that the BO coating did not fully alleviate the effect of high surface traction and the subsurface WECs and butterfly wing cracks initiated by non-metallic inclusions and micro cracks still occurred.

Keywords: wind turbine gearbox bearing; black oxide coating; white etching crack; non-metallic inclusion

1 Introduction

Premature failure of wind turbine gearbox (WTG) bearings has been a cause of concern in wind turbine field operation. The mechanism by which WEC damage leads to WTG bearing failure is the subject of intensive research by both industry and academia; however, its root causes and damage initiation mechanisms have yet to be fully understood. Although many bearing failure modes have been reported, it has been widely acknowledged that the premature failure of WTG bearings is mainly caused by the White Etching Cracks (WECs) associated with microstructure alterations termed as the White Etching Area (WEA) [1][2][3].

The WEA is a microstructure alternation that can be observed around an inclusion or a void or along a

found that the grain size of the WEA varied according to the distance from the associated micro crack which was 10 to 100 nm when close to the crack but was 0.5 to 1 µm at the boundaries of the butterfly wing. It was also found that there were two regions within WEA in WECs, one was associated with a nano-crystalline body centred cubic (bcc) ferrite, and the other with a mixture of the nano-crystalline bcc and newly formed metastable carbide M_2C structures [12]. When the WEA was observed around a non-metallic inclusion, a butterfly shape was often seen with one or more wings, which were created by WEAs [10][13]. Recently, an Atomic Force Microscopy (AFM) scanning of the WEA in the butterfly wings had revealed that the WEA was a damaged material at the debonded gap between inclusion and steel matrix [14]. The relation and sequence of formation of WEAs and WECs are not fully understood and an agreement has yet to be established regarding the root causes of the WEC/WEA initiated WTG bearing failure. However, a number of hypotheses had been proposed regarding the key initiation factors of WECs/WEAs, such as the influence of non-metallic inclusions [9][10][13][15][16] [17][18], the amount of retained austenite [19], the type of lubricant used in operation and consequently the amount of hydrogen generated [4][5], as well as levels of Hertzian contact stress induced by overloading conditions [18][20][21][22], effects of under loading [23], surface sliding between bearing rollers and raceways, and dynamic and transient loading conditions of wind turbine operations [5][7][16][24][25] [26][27].

According to the subsurface damage initiation mechanism, the WEAs could be initiated around non-metallic inclusions, which formed butterfly wings, and further developed into WECs [10][13]. These inclusions, such as Manganese Sulphide (MnS) or Aluminium Oxides (Al_2O_3), could be either softer or harder than the bearing steel matrix [28]. However some researchers suggested that WECs were surface initiated [20] and their propagation was influenced by oxygen ageing components of the lubricants and hydrogen, combined with effect of loading and environmental factors [29]. Other initiation factors could be the impact loading or vibration-related conditions [30]. The initiation mechanism of surface initiated WEC was explained by tensile stress due to high traction on the surface, which initiated brittle fracture cracks on the surface which then propagated into subsurface due to corrosion-fatigue cracking, caused by hydrogen penetration into the initiated crack. This mechanism suggested surface top-down crack propagation into the subsurface [6][20][29][31].

Surface treatments had therefore been proposed by bearing manufacturers to protect roller bearings from surface initiated damage due to WTG bearings operating in the mixed or boundary lubrication regimes [32][33][34]. Another advantage claimed for applying some coating to bearing surface was to reduce hydrogen absorption and prevent subsurface initiated embrittlement leading to cracks/WECs

Black oxide is a chemical conversion of the bearing steel surface and it is normally applied on bearing rollers and raceways. This layer is formed by immersing the part in chemical solutions, mainly an alkaline aqueous salt solution, for specific time at temperature between 130 and 150 °C with 15 steps of immersion [34]. The resulted black layer is Fe_3O_4 (a blend of FeO and Fe_2O_3), which is reported to have lower hardness than the bearing steel matrix and a thickness of approximately 1-2 µm [34]. This technology has been reported to reduce friction [36], and is well known for reducing corrosion.

Experimental work using a ring-on-ring tribometer tester was conducted by Evans et al. [33] to investigate the adhesive wear resistance of a BO layer and a Diamond-Like Carbon coating WC/a-C:H. The BO layer in their study was formed by using a single-bath process. The test results showed that BO layer provided lower adhesive wear protection compared to the WC/a-C:H. Another test conducted by the same research group used tapered roller bearings made of case-carburized quality low-alloy bearing steel. Two sample groups of bearings were tested with four bearings in each sample group. Again, one group of the bearings was coated with BO and the other group with WC/a-C:H. The fatigue life of bearings in these sample groups was obtained using a first-in-four life test procedure, where the life was measured as the time at the occurrence of a first spall greater than 6 mm^2, which was detected by a vibration sensor. The contact pressure between roller and inner raceway during the tests was ~2.4 GPa with a lambda ratio 0.5~1, determined based on the initial roughness of the contacted surfaces. The results showed significant improvements in bearing life due to the use of WC/a-C:H, almost eight times the life of the uncoated bearings, while a very slight extension in bearings life was observed from the bearings with BO coating. However, two issues in sample preparation procedure led to a conclusion that these results were not directly comparable. Firstly, the single bath process to form the BO layer in the reported study could not produce specifications of the BO layer similar to that formed by the 15 steps of immersion procedure adopted by WTG bearing manufacturers. Secondly, the bearings used in the tests were case-carburized, while most bearings used in WTG were through hardened, thus the results of fatigue life may not be exactly the same. Despite some questions remain regarding the results obtained in the reported studies, the investigations highlighted the need to further examine the effectiveness of BO coating for prolonging the life of WTG bearings.

Another study reported the comparison of the WEC initiated failure among bearings with case carburizing and BO coating [37]. The study was based on observing a number of WTG bearings in field operation for 14 months, and it showed that bearing failures by WECs dropped from 40% to 2.7% after replacing the bearings without surface treatment with case carburized bearings [37]. The same

zero percent failure by WECs was reported at 26 months in the field operation, a longer monitoring period was needed to fully assess the effectiveness of surface treatments to prolong the bearing life. The study compared three different surface treatment solutions to tackle the WEC initiated failure. However the most commonly adopted surface treatment method for WTG bearings is the BO coating, because it is less expensive than other surface treatment methods. Despite using BO coated bearings in WTGs the premature bearing failure by WECs is still being reported, an example of such failure will be examined in this study to characterise both surface and subsurface damage features and to investigate potential damage initiators.

This study presents a damage investigation of a failed BO coated planetary bearing retrieved from the gearbox of a multi-megawatt wind turbine. The investigation consisted of a metallurgical damage examination and BO layer characterisation. The examination focused on characterising the initiation of both surface damage and sub-surface damage associated with non-metallic inclusions. In order to characterise the subsurface microstructural defects associated with non-metallic inclusions, steel cleanliness of the BO bearing was examined. To evaluate the mechanical properties of BO coating layer, hardness, modulus of elasticity and thickness of the BO layer in damaged and undamaged raceway surface regions were measured by using Nano-indentation technique. Various forms of microstructural damage were observed in the BO coated bearing, which were compared with the microstructural damage observed in the uncoated bearings investigated in our previous published studies [13][14][38].

2 Experimental Procedure

2.1 Sample Sectioning

The examined inner raceway of the BO coated bearing had severe surface damage in the loaded zone, with a band covered the entire width of the raceway, except the edges under the cage, and extended to 220mm in length along the raceway circumference, as shown in Figure 1. Along this band, the BO coating had been completely removed. Outside the severe damaged region of the loaded zone, in the vicinities close to the entrance and the exit sides of the loaded zone of the raceway, the visual examination revealed that the BO layer was slightly removed. Various sized indents, which could be produced by debris carried from the severe damaged region, were seen over almost the entire raceway circumference outside the loaded zone. However, the indents had a higher density and greater size (more than 3mm in maximum dimension) at the exit side of the loaded zone when compared with those at the entrance side to the loaded zone.

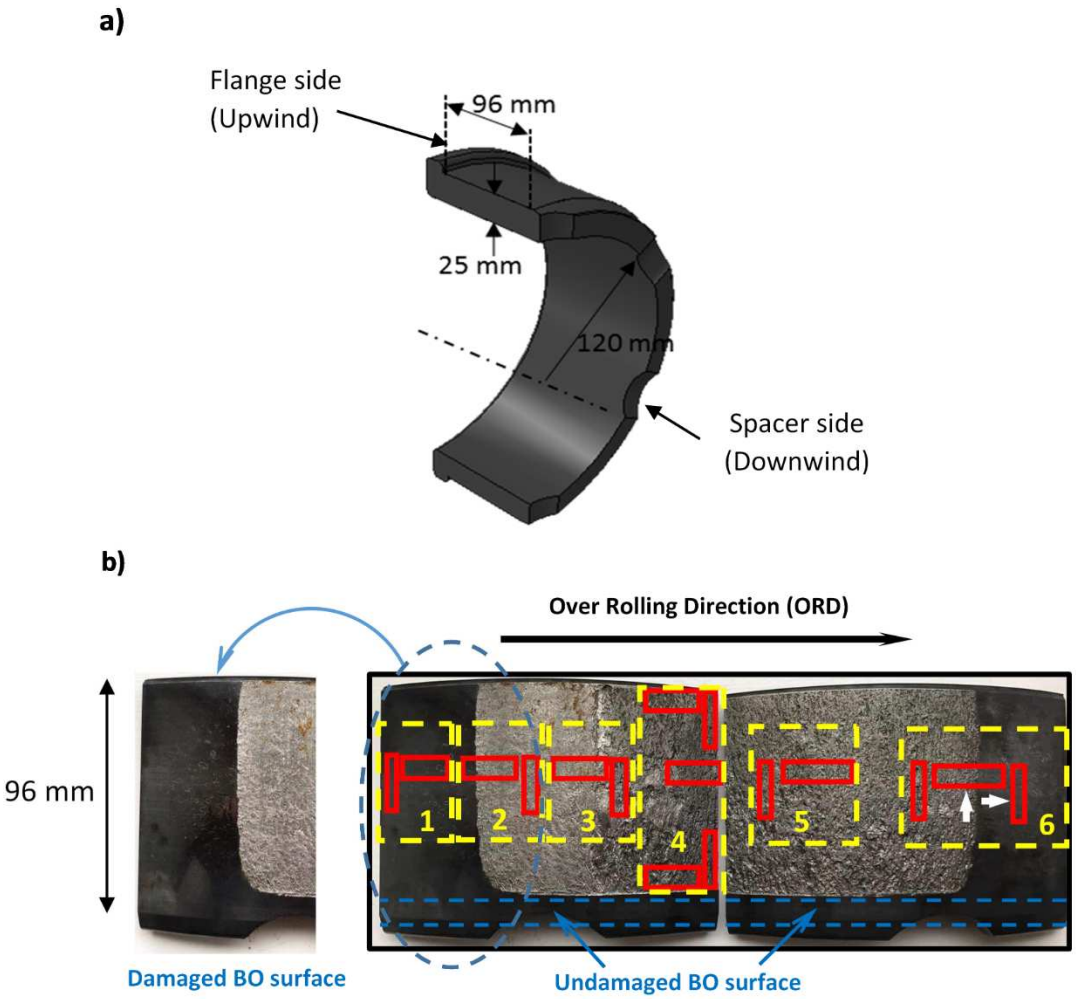

Figure 1: (a) Dimensions of the examined BO bearing (b) Sectioning of the inner raceway: locations of samples (shown as red blocks) – 8 for observation in the axial direction and 8 for observation in the circumferential direction (shown by white arrows), covering 6 regions (shown by yellow boxes).

2.2 Sample Preparation for Microscopy

A wire erosion machine was used to cut the samples from the BO bearing inner raceway shown in Figure 1 and to reduce the thickness of the samples which were further sectioned to a 2-mm thickness by using an abrasive cut-off wheel and automatic cutter. The samples were then hot mounted using the mounting material Bakelite for optical microscopy and conductive Bakelite for Scanning Electron Microscope (SEM). Grinding and polishing were applied to the mounted samples by using an automated grinding and polishing machine. After grinding and polishing, the samples were etched with 2% nital to reveal the microstructure alterations such as WEAs. Using optical

2.3 Steel Cleanliness Examination

To investigate the subsurface inclusion-initiated damage, the examination of the steel cleanliness of microstructure of the BO bearing was necessary. The examination was conducted using methods recommended in ISO-4967 [40], where non-metallic inclusions were classified into Types A (sulphide), B (aluminate), C (silicate), D (globular oxide) and DS (single globular). The axially sectioned samples were chosen for cleanliness examination because longer inclusions were expected to be found, representing the worst cleanliness condition (highest number and biggest size of inclusions). The size and number of each inclusion type found were recorded and each inclusion was classified into a fine or thick series according to limits provided in ISO-4967. The length of inclusions from the same type and thickness series were summed up and the total length was then converted into an index number, representing a cleanliness rating according to ISO-4967. Inclusions of all sizes were considered for calculating the total length of inclusion Type A, B, C and D respectively. Table 1 shows the index numbers of different inclusion types and the average and worst cleanliness ratings of the BO bearing steel. Their comparisons with the required cleanliness ratings for through hardened bearing steels defined in the international standard ISO683-17 [41] is also presented. It can be seen that the cleanliness of inclusion Types A, B and C were sufficient according to ISO 683-17 however inclusion Type D had an index number greater than the rating specified by the standard thus did not meet the required cleanliness requirement.

Table 1: Steel cleanliness rating in axially sectioned samples of BO coated bearing

Cleanliness of BO coated bearing	Type of non-metallic-inclusions [40]								
	A		B		C		D		DS
	Fine	Thick	Fine	Thick	Fine	Thick	Fine	Thick	
	Index numbers for different types of inclusions								
Average cleanliness	0.3	0.2	0.2	-	0.1	-	2.0	0.2	-
Worst cleanliness	0.5	0.5	1	-	0.5	-	2.5	0.5	-
Required cleanliness [41]	2.5	1.5	2	1	0.5	0.5	1	1	2

2.4 Energy Dispersive X-ray Analysis (EDXA)

In addition to the cleanliness analysis, EDXA was conducted on a number of inclusions which developed subsurface WECs and butterfly wings. The EDXA confirmed the high content of chemical elements of inclusion Type D. However, not only Type D inclusions were found to initiate subsurface damage but Type A and compound inclusions, which had the chemical compositions of more than one type of inclusions, were also found to initiate WEC/WEA damage. EDXA results of some selected inclusions will be presented in Section 3.1

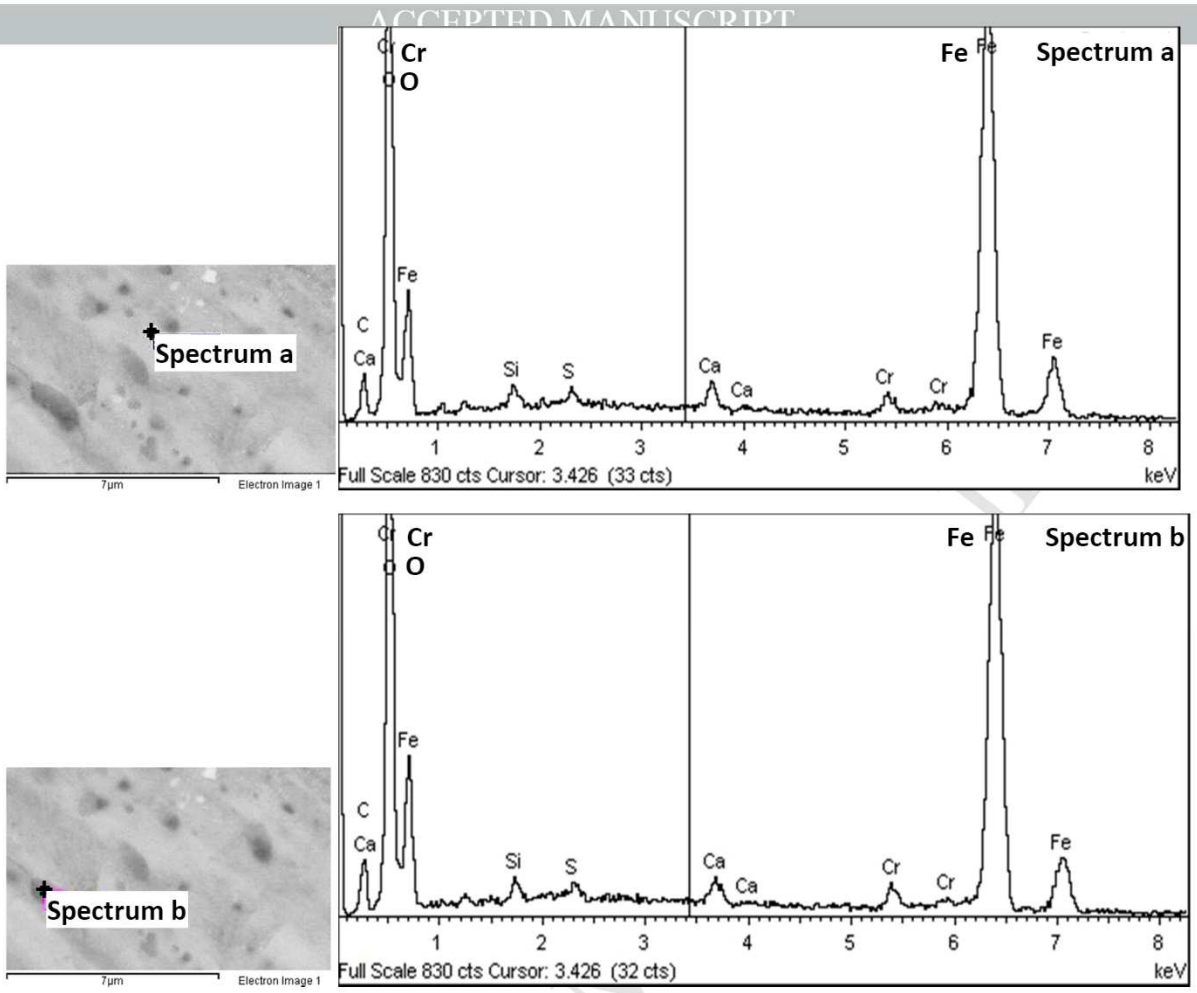

Figure 2: EDXA of the undamaged region of BO layer at the side of the raceway

EDXA was also used to view the chemical composition of the BO layer, as shown in Figure 2. The analysis was conducted on the undamaged region of the BO layer at the side of the raceway, as shown in Figure 1. Because the X-ray can penetrate the very thin BO layer, Figure 2 shows mainly peaks of iron oxide and other chemical elements existed in the bearing steel such as Cr and Si. Dark spots appear in the SEM images of this layer, which have a similar spectrum of chemical elements as the rest of the BO layer, by comparing the two spectrum diagrams in Figure 2. Accordingly, these dark spots indicate the porosity of the oxide.

2.5 Nano-indentation Test

Nano-indentation technique was applied to measure hardness and thickness variations of the BO layer on damaged and undamaged regions of the bearing raceway surface. These measurements were essential to potentially evaluate the effect of loading conditions on the BO coating layer therefore damage occurred when the bearing was in service. The measurement was firstly conducted

layer was softer than the steel matrix and it was significantly removed at the region of the entrance to the loaded zone. In order to measure the entire intact BO layer, a higher load than the maximum capacity of 10mN had to be applied. Further Nano-indentation test was conducted by using Hysitron TI Premier, which covered a wider range of load cycles than that of the Hysitron Triboscope. The results of Nano-indentation tests and the relevant measurement details to characterise the BO layer will be presented in Section 4.

3 Damage Evaluation and Characterization

In this study of a BO coated bearing, various forms of microstructural damage were found from the metallurgical examination. These were

(a) inclusions initiated WEAs in the form of butterfly wings,
(b) WECs,
(c) subsurface micro-crack that were not connected to the surface but could be linked to inclusion(s),
(d) surface-breaking RCF cracks that were connected to the surface and had a specific inclination but not linked to inclusions.

Representative images of these observed forms of microstructural damage are shown in Figure 3. These forms of damage in the BO coated bearing were similar to those observed in the uncoated planetary bearings from our previous studies published in [13][14][38] which focused on investigating subsurface initiated damage. In sections 3.1, 3.2 and 3.3, the microstructural damages in the forms of butterfly wings, subsurface cracks, and surface breaking cracks will be discussed in detail.

To characterise damage features of the butterfly wings and micro-cracks initiated from inclusions, angles of the inclusion, right and left cracks or butterfly wing cracks relative to the Over Rolling Direction (ORD) were measured. Their definitions are shown in Figure 4(a). For the inclusions, the length was measured by the distance between the inclusion tips, or the radius for globular inclusions, the width was measured by the distance perpendicular to the length of the inclusion, and the depth was measured from the bearing raceway surface to the centre of the inclusion. The length, width, depth and angles of cracks of inclusions and WEAs in the axially and circumferentially sectioned samples were recorded for analysis.

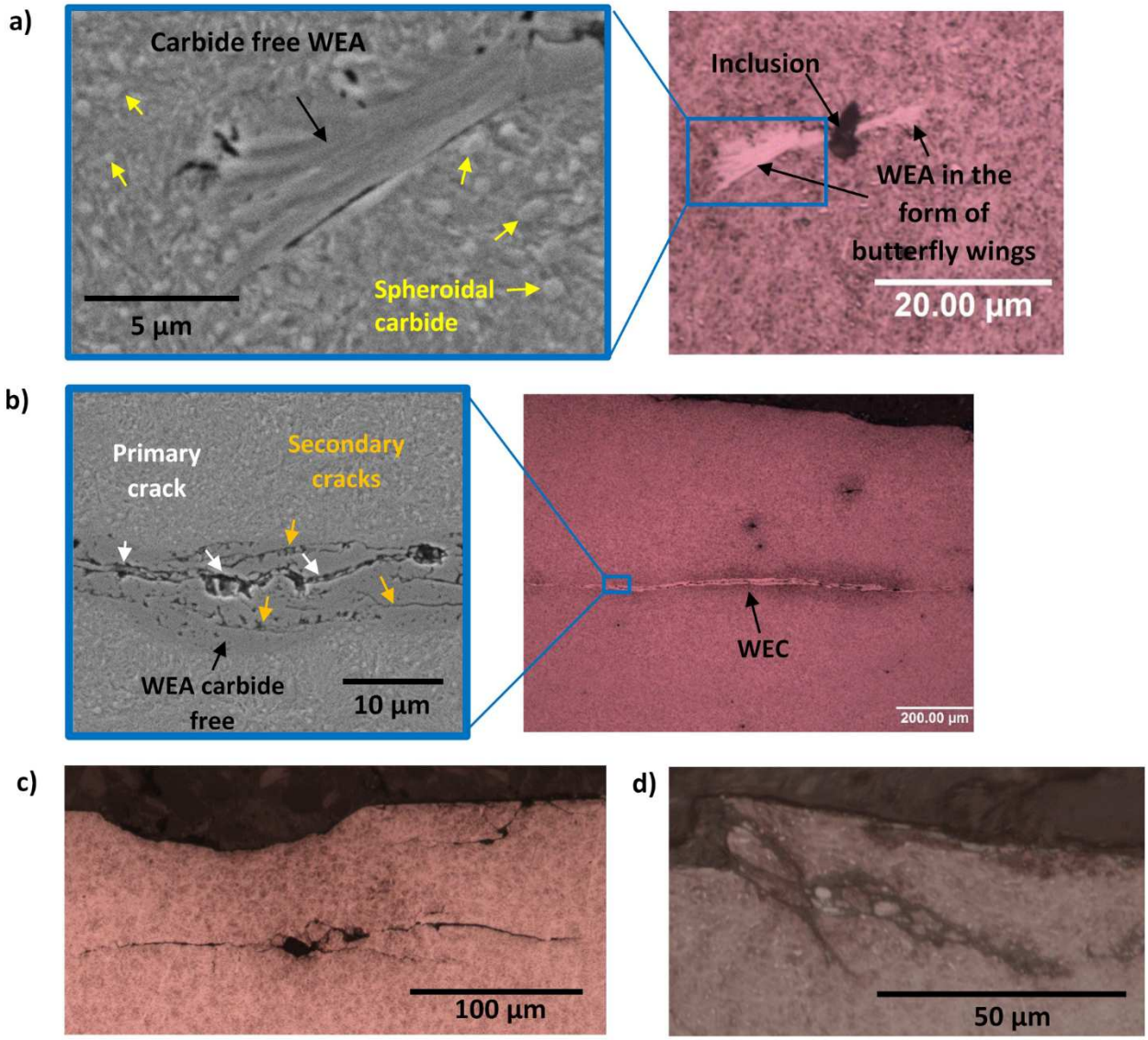

Figure 3: Examples of different forms of microstructural damage in the BO coated bearing: (a) Butterfly wings; (b) WEC; (c) Subsurface cracks in the axially sectioned sample; (d) Surface-breaking RCF cracks.

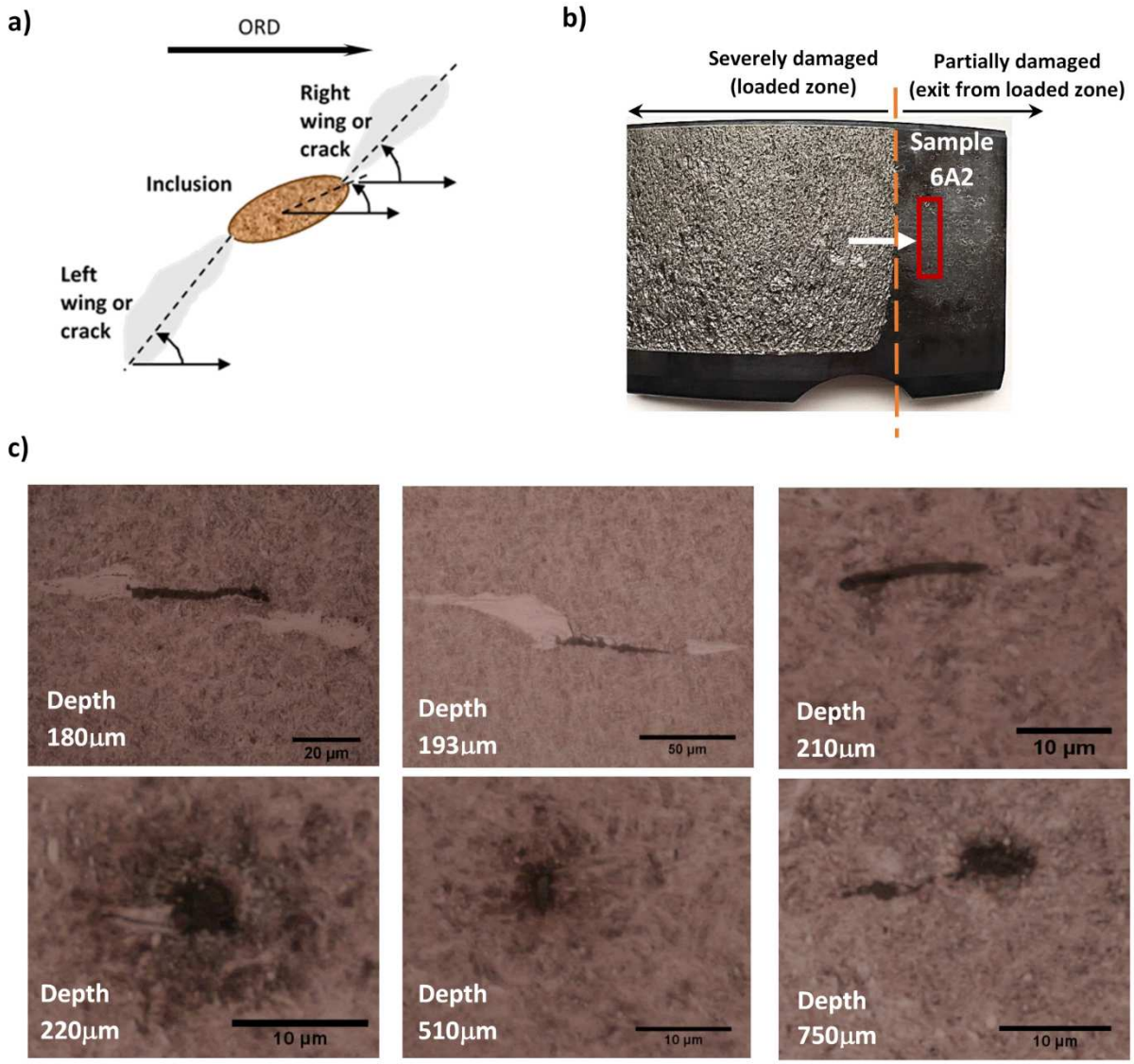

Figure 4: Inclusion initiated damage: a) Definition of angles of inclusion and butterfly right and left wings; b) Sample 6A2 axially sectioned sample located at exit region to loaded zone; c) Examples of butterfly wings initiated at inclusions and their depths.

3.1 Butterfly wings

In this bearing, the inclusions associated with butterfly wings were mostly Type D inclusions (65% of all inclusions observed). The total number of butterflies with single and double wings observed in the circumferentially and axially sectioned samples was 28. The characteristics of the butterflies and their initiating inclusions are shown in Figure 5, which are compared with that observed in the uncoated WTG bearings in one of our previously published studies [14]. Despite being different in sizes between the two bearings, the characteristics of the observed butterflies in both bearings showed

bearing in both circumferential and axial sections despite the BO bearing has shorter average lengths of inclusions. In addition to the inclusion size, the inclination of the inclusions is different in both bearings as shown in Figure 5(c). The variation in the size and inclination of inclusions could be due to the different sizes of bearings and different inclusion types where Type D was the dominating damage initiating inclusion type in the BO coated bearing. This inclusion type has different aspect ratios when comparing to that of Type A inclusions (MnS) in the uncoated bearings of our previous study [14]. The difference in the size of butterfly wings could be due to the different number of cycles and loading levels experienced by each bearing. Figures 5(c) and (d) show that in both bearings the inclination angles of the butterfly wings are less than the angle of the maximum shear stress, 45°, indicating the effect of surface traction on the formation of the observed butterflies in both bearings, as depicted in Figure 6. This provided an evidence indicating that the BO coating had not prevented the formation of the butterfly cracking initiated at inclusions despite its intention was to reduce hydrogen absorption and prevent bearing subsurface initiated embrittlement leading to cracks/WECs.

A high number of butterflies at inclusions was observed in Sample 6A2 (shown in Figure 4(b)), which was the vertically cut sample on the right-hand side of Region 6 located at the exit from the loaded zone (shown in Figure 1). Some examples of damage initiating inclusions found in this sample are shown in Figure 4(c). An inclusion located at a subsurface depth of 750∝m had micro-cracks propagated from an inclusion and the inclusion at depth of 510∝m had separation but without butterfly wings, while all other inclusions at various depths, shown in Figure 4(c), were associated with butterflies. The butterfly of the inclusion at depth 193∝m had the longest wings among all other butterflies observed in this sample. In this sample, the layer of the BO coating was not completely removed but the surface showed many big indents (more than 3mm in maximum dimension). The indented surface was observed by the metallurgical examination as a concave surface without any surface linked cracks, which was different from another vertically cut sample on the left-hand side of Region 6 located within the loaded zone, shown in Figure 1. This indicated that the bearing might have experienced high levels of loading and surface traction during its operation that led to the initiation of micro cracks and butterfly cracks in greater depths when the BO coating on the raceway surface was still partially intact. It provided further evidence that there were multiple initiators leading to the WEA/WEC microstructural damage.

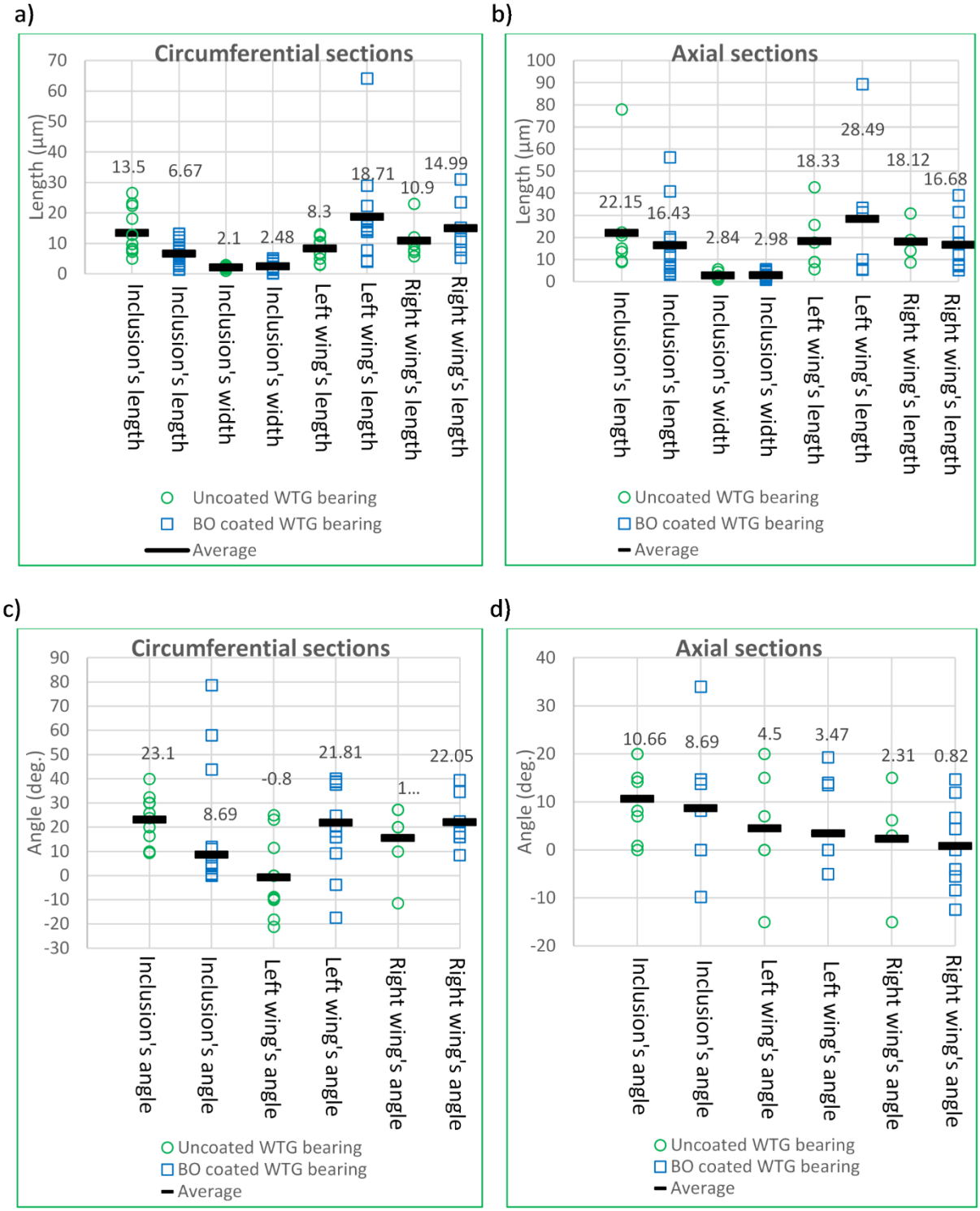

Figure 5: Characteristics of the observed butterfly wings and their initiating inclusions in the BO coated bearing and the previously examined uncoated bearing [14] **(the number above each characteristic refers to the average value): (a) length of inclusions and butterflies wings in circumferential sections; (b) length of inclusions and butterflies wings in axial sections; (c) inclination angle of inclusions and butterflies wings in circumferential sections; (d) inclination angle of inclusions and butterflies wings in axial sections**

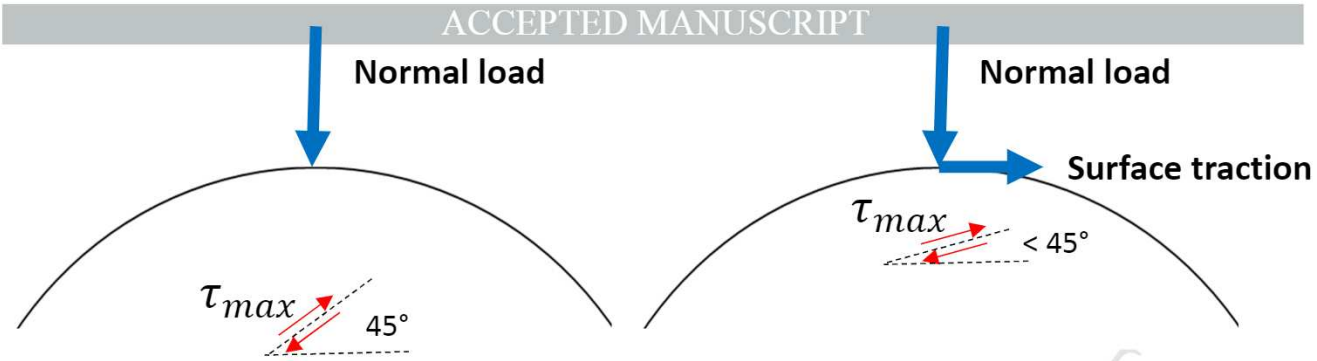

Figure 6: Illustration of the effect of surface traction on the inclination of maximum shear stress and thus butterfly wings angles and damage location in subsurface

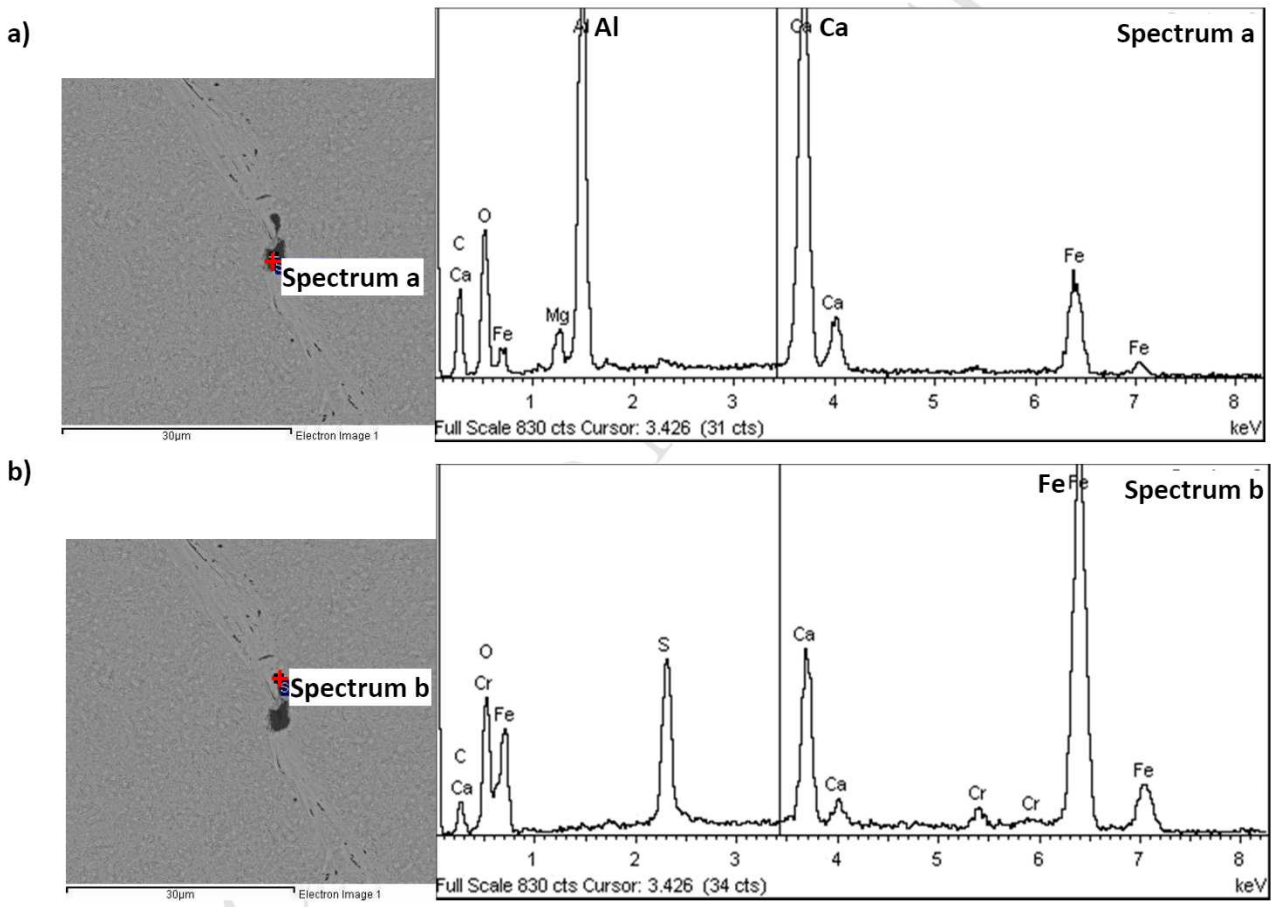

Figure 7: EDXA of the inclusion that initiated the longest butterfly in a circumferentially sectioned sample

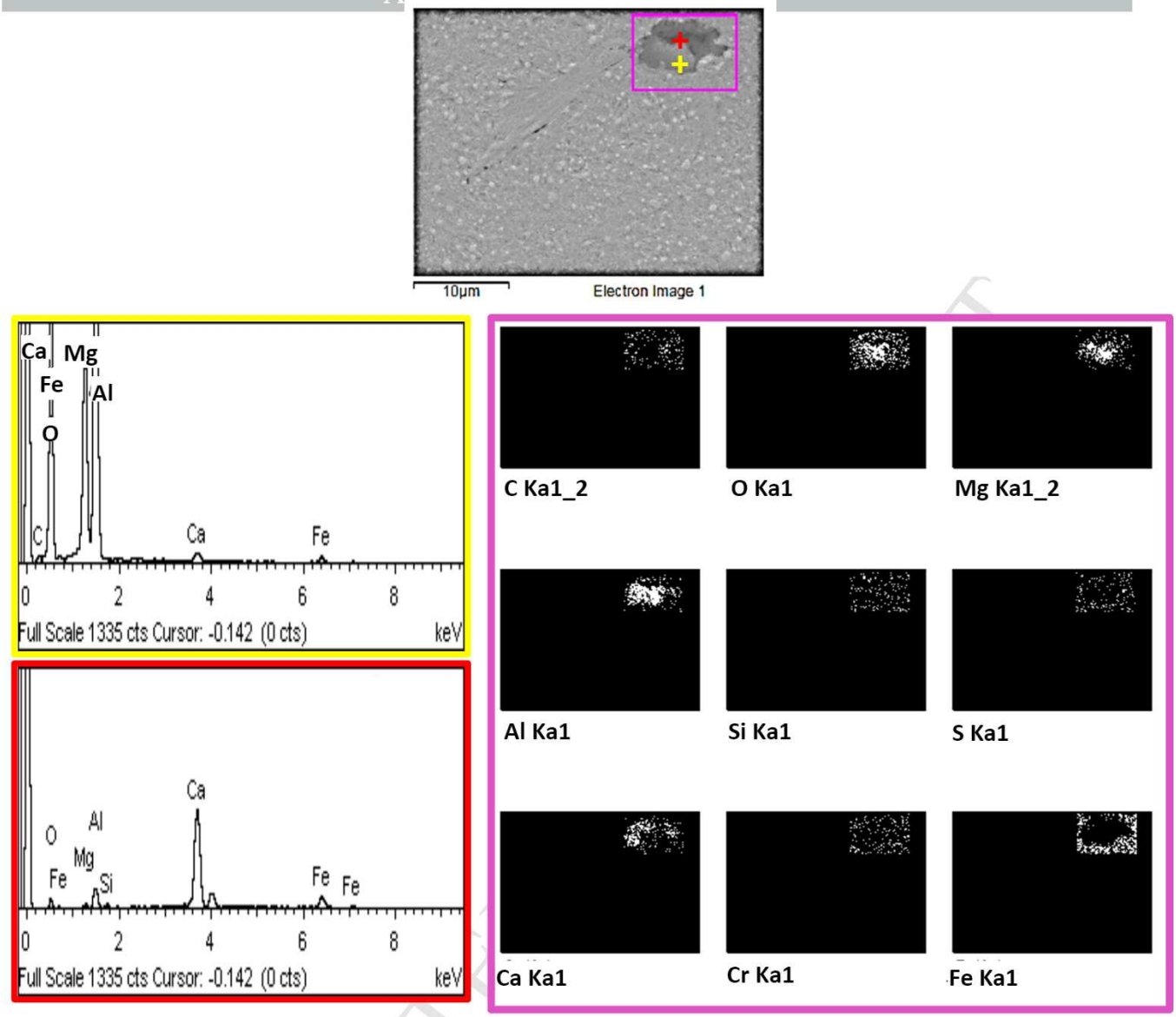

Figure 8: EDXA of chemical elements of Mg-Al-O inclusion

The EDX analysis of the inclusions that initiated most of the butterflies revealed they contained the chemical elements similar to those of Type D inclusions. However, some of the inclusions showed chemical elements of a soft sulphide inclusion adjacent to a hard oxide inclusion, as can be seen in Spectrums shown in Figure 7, with an aspect ratio <3 that matches Type D inclusions. The longest butterfly found from a circumferentially sectioned sample had this combination of inclusions, the only one found. This butterfly was found in a sample taken from the raceway edge on the flange side, the top sample horizontally cut from Region 4, as shown in Figure 1. To show the distribution of chemical elements of the inclusion, EDXA mapping was conducted and shown in Figure 8. It shows that the key chemical elements to form one of the four types of inclusions (Types A, B, C, D) were

nucleation of the carbide [39]. Thus, this type of inclusions would most likely contribute to the formation of the WEA, since this microstructure alteration is characterised by the dissolution of carbide.

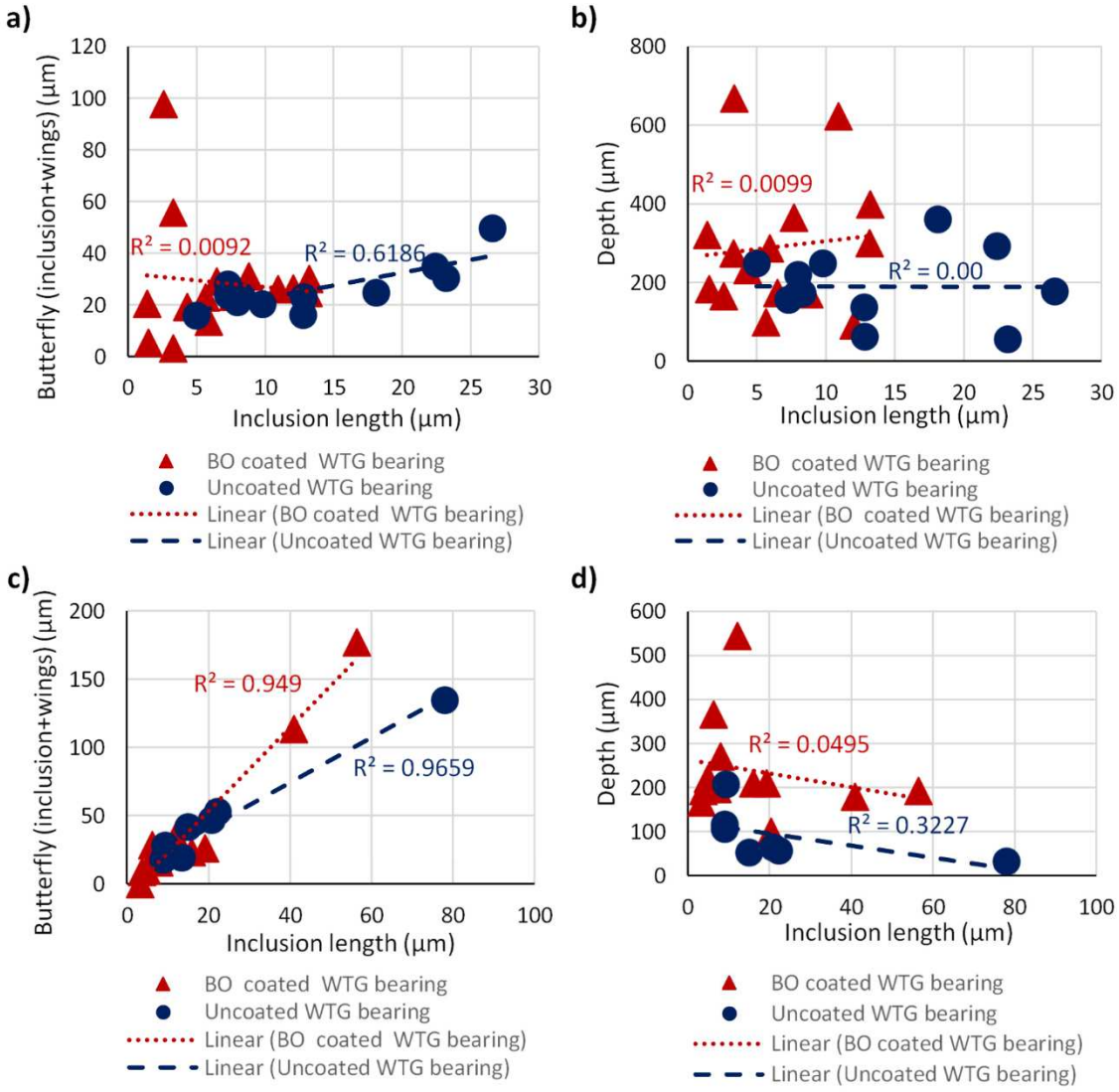

Figure 9: Inclusion length vs. total butterfly length and Inclusion length vs. depth of inclusions: (a) and (b) butterflies in circumferentially sectioned samples (c) and (d) butterflies in axially sectioned samples.

Figure 9 shows the relations between total butterfly length (inclusion length + butterfly wing length) and inclusion length in circumferentially and axially sectioned samples from the BO coated bearing investigated in this study and the uncoated bearing investigated in the previous study [14]. Figure 9(a) shows that the relation between the butterfly length and inclusion length in the BO coated bearing circumferentially sectioned samples is not similar to that in the uncoated bearing. The difference of the dominant inclusion types, thus different inclusion aspect ratios, in each bearing can

conclusion can be supported by the results shown in Figure 9(c) where a very clear relation exists between butterfly length and inclusion length in the axially sectioned samples since the inclusion lengths in the axially sectioned samples are much greater than that in circumferentially sectioned samples. Although Figures 9(b) and (d) show similar trends for the relation between inclusion length and butterfly depth in both coated and uncoated bearings, these relations are not strong. In addition, no assertive conclusions could be made about the effect of inclusion depth on the total length of butterfly. These observations and analysis from Figure 9 show similar trends of the effect of inclusions on butterfly formations for both the BO coated bearing and previously investigated uncoated bearing [14]. This indicates that the BO coating layer was ineffective in alleviating the effect of non-metallic inclusions on the subsurface initiated damage of micro-cracks and butterflies.

3.2 Subsurface cracks

Some of the observed cracks in the circumferentially and axially sectioned samples were not linked to the surface. They could be either a single crack or a network of cracks in subsurface and there were different characteristics between circumferentially and axially sectioned samples.

In the circumferentially sectioned samples, the subsurface cracks had irregular shapes. Some of the cracks were found to attach to inclusions that propagated almost vertically to the contact surface, an example is shown in Figure 10(a). The crack could be initiated from the inclusion shown or another inclusion, since the crack was completely under the surface and the only stress concentration point found along the crack was this inclusion. There might be another inclusion where the crack could initiate from, which might have been removed during the sample preparation process, or it could be behind the examined surface of the sample. The EDX analysis of this inclusion shows it was a MnS inclusion, even though Type D inclusions were the dominating type inclusion initiating most damage in this bearing. However, without examining the entire inclusion of 3D in shape including the part under the examined surface or the part that might have been removed by sample preparation, it could not be confirmed that the inclusion was a pure manganese sulphide since it could be aluminates embedded in manganese sulphide [40][41].

The subsurface cracks observed in the axially sectioned samples showed consistent features. They were mostly flat, parallel to the contact surface, and some ends of the cracks were inclined to the surface at a specific angle, an example is shown in Figure 10(b). It was found that the inclination angle was shallow, about 15° to the bearing axis. These cracks could propagate toward the surface to form the subsurface initiated spalls on the surface. It was found that the depth of some of the WECs were

without WEA if the stress and loading cycle levels required for phase transformation were not reached during loading. Again, these observations provided evidence showing that the BO coating could not prevent the subsurface initiation and propagation of micro cracks and butterflies leading to surface spalling. This limitation of the BO layer will be discussed in the measurement results of the mechanical properties of the BO layer in Section 4.

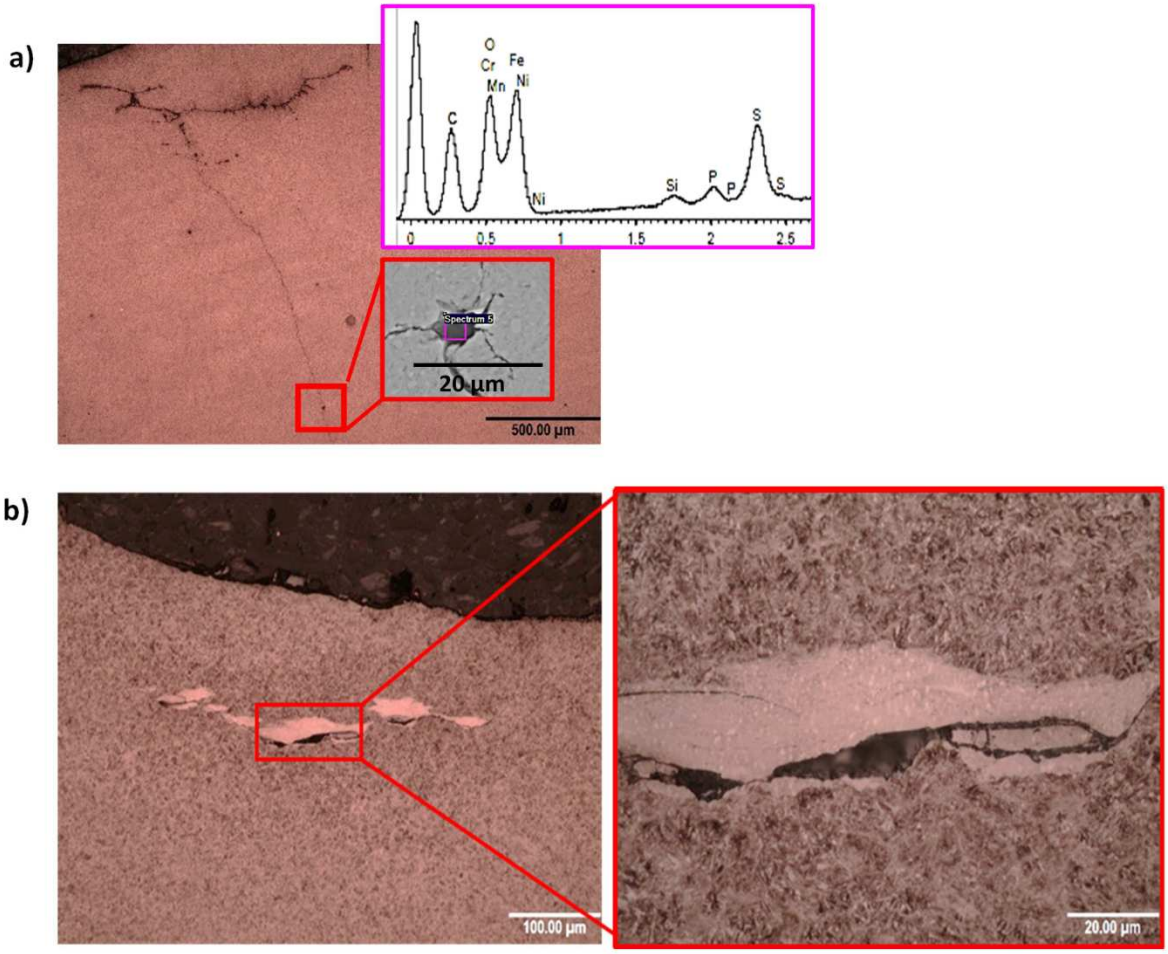

Figure 10: (a) Subsurface crack network initiated from an inclusion at depth>1500µm, in a circumferentially sectioned sample; (b) Subsurface WECs in an axially sectioned sample.

3.3 Surface Breaking Cracks

Some of the cracks linked to the surface showed similar characteristics, for example the inclination of the cracks. In some of these cracks, fragments of steel particles were confined within the space created by a crack, as shown in Figures 11(a) and (b). For some surface-breaking cracks the colour of these confined particles appeared to be similar to the WEAs attached to the WECs, especially when they had propagated from the surface into deeper locations, as shown in 11(d), which can be

subsurface initiated cracks, the stress concentration around the debonding between the non-metallic inclusions and the steel matrix might have initiated the cracks due to the cyclic loading and the developed tension and compression stresses around inclusions.

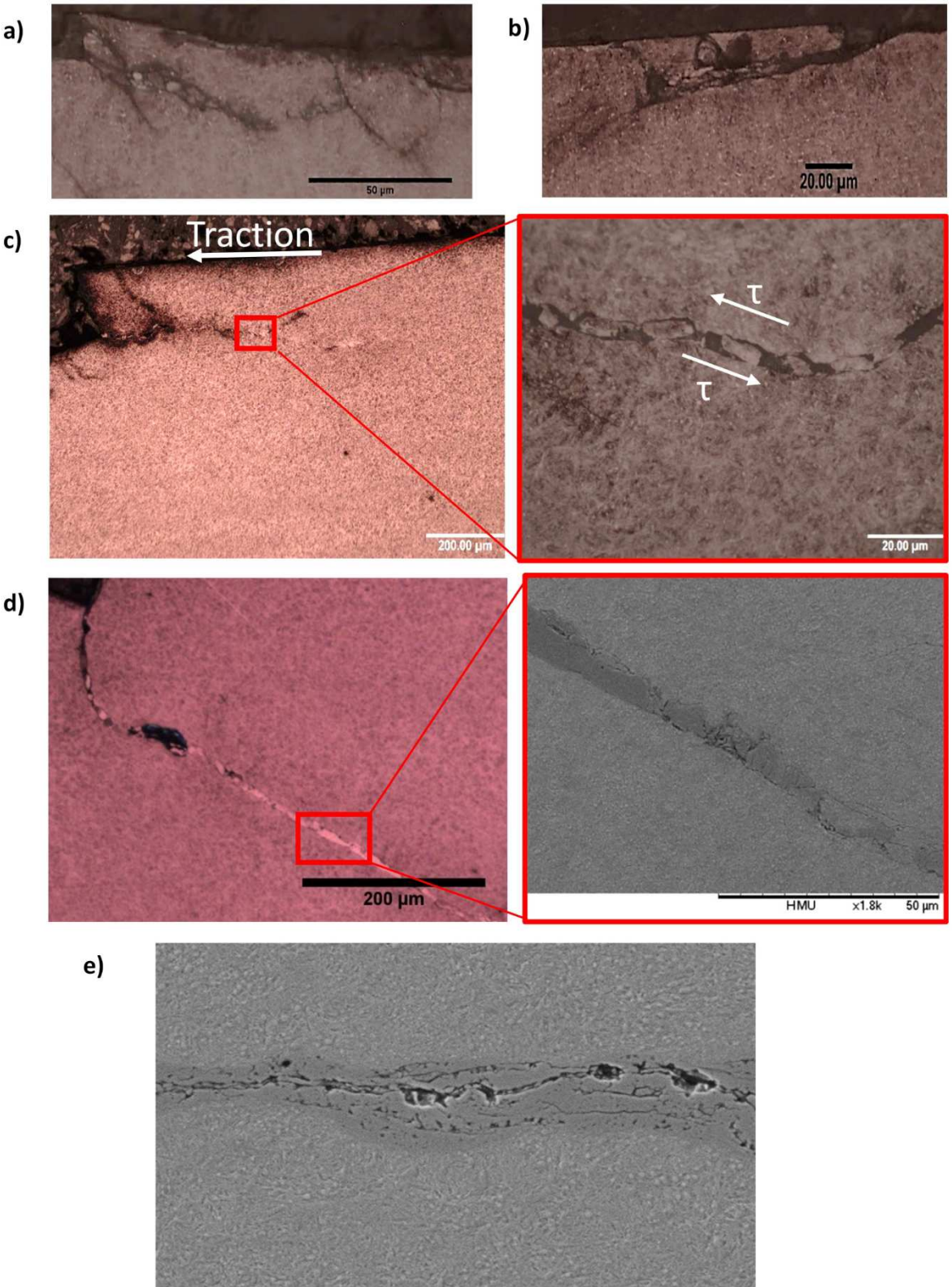

Figure 11: Surface-breaking RCF cracks: (a), (c) and (d) surface-breaking RCF cracks in circumferentially sectioned samples; (b) surface-breaking RCF cracks in axially sectioned sample; (e) WEC from an axially sectioned sample appeared to be similar to surface-breaking RCF crack in (d).

The inclination angles of the surface-breaking RCF cracks in the axially sectioned samples were similar to those of the subsurface cracks. This indicated that the cracks had propagated almost at the same angle in the axially sectioned samples regardless of their initiation locations, either surface or subsurface. The surface-breaking RCF cracks that initiated from the surface and propagated downward were found to turn upwards after a certain distance, generating surface spalling or micropitting, an example is shown in Figure 12(a). Relatively small spalls or pits were generally formed by surface-breaking RCF cracks, then from these spalls other cracks started propagating downwards and forming bigger spalls, as shown in Figures 12(b) to (d). It was possible that the BO coating provided benefits protecting the raceway surface to a certain extent however this examination showed that the BO layer did not fully alleviate the effect of surface initiated damage which caused severe spalling.

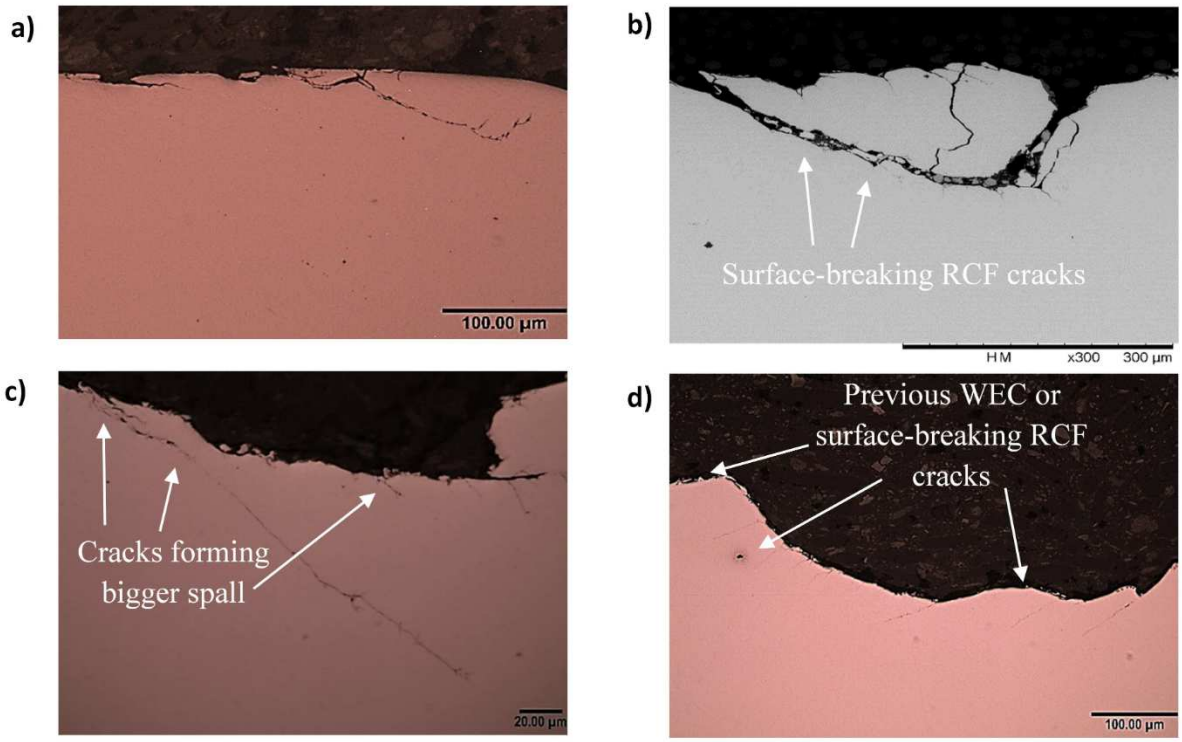

Figure 12: Surface cracks: (a) crack changed direction toward the surface to form a spall; (b) to (d) stages of spall formation by surface-breaking RCF cracks, in circumferentially sectioned samples.

4. Characterisation of Black Oxide Coating

As described in Section 2.5, two Nano-indentation systems, Hysitron Triboscope and Hysitron TI

indentation, using a three-sided 120-degree Berkovich indenter tip to apply a load and to simultaneously measure the displacement. The Nano-indentation test was performed by applying and removing the load. The unloading part of the load-displacement curve was used to find the hardness H and the reduced modulus of elasticity E_{r}. The modulus of elasticity for the diamond indenter was 1120 GPa and the Poisson's ratio was 0.07 which were used with E_{r} to calculate the E value of the indented material. In the measurements using Hysitron Triboscope the maximum load of 10mN was applied in 25 steps of loading-partial-unloading for each indent. In this kind of loading cycle, for each indent, the total load was applied incrementally through a number of steps. At each cycle, the load reached a maximum value followed by holding then unloading to a specific percentage of this maximum value of load at the current step. From each cycle of loading-partial unloading, H and E_r were determined. Accordingly, for each indent into the running surface there were a number of measurements for H and E_r equal to the number of loading-partial unloading steps, and each of these values represented the Nano-mechanical property at a certain depth which were plotted as shown in Figures 13(b) and (c). Because of more than one indent was considered in the measurement, the mean value was determined with error bars showing standard deviations.

The loading-partial unloading technique described above allowed the measurements of the hardness and modulus of elasticity at different depth, an adopted technique to measure the properties and thickness of coatings and graded materials in [42][43] including the BO layer [33]. To determine the thickness of the BO layer, the subsurface hardness of the examined bearing was needed as the hardness of the bearing steel may differ from one bearing to another. For the examined BO coated bearing, a sample was sectioned from the undamaged BO region as shown in Figure 1. After grinding and polishing, the subsurface hardness was measured using the microindenter Durascann and the average hardness for 18 indents was found to be HV0.3 = 748.5, equivalent to 7.34 GPa.

For the low load test using Hysitron Triboscope, the indentation pattern used was a matrix of 3×3 indents with 15 µm spacing, as shown in Figure 13(a). The maximum indent size was 1.6 µm for the partially removed (damaged) region and 2.2 µm for the undamaged region of the BO layer. The sample used to measure the thickness and Nano-mechanical properties of a partially removed BO layer was taken from the entrance region to the raceway loaded zone, which was inside Region 1 in Figure 1(b). The Nano-indentation test on the surface of this sample showed a very thin BO layer, as revealed by the depth values in Figures 13(b) and (c). The hardness and modulus of elasticity of the steel matrix could be seen at the end of these curves indicating the end of the BO layer thickness. However, the Nano-indentation on the surface of a sample from the undamaged BO region, shown in

In order to measure the entire thickness of the undamaged BO layer, higher loads were applied using the Nano-indentation system Hysitron TI Premier with a three-sided 120-degree Berkovich indenter tip. In this test, four indents were made using a maximum load of 1000 mN, divided into 20 cycles of loading-partial-unloading. The pattern of indents was a 2×2 matrix with 150 µm spacing and the maximum indent size was 20 µm. The variation of the hardness and modulus of elasticity through the whole thickness of the undamaged BO layer is shown in Figure 14. Considering the size of the indents and sufficient distance between the centres of the indents, much higher than the recommended 3 times of the indent size, the effect of the indent size on the measurement was minimised.

Figure 14(a) shows that the end of the BO coating layer is around 2.2 µm in depth from the surface where the hardness of the bearing steel is reached. This thickness is very close to the 2 µm reported by a bearing manufacturer [29]. Previous study reported by Evans et al. [33] investigated the effect of BO coating on the performance of bearing steel during bearing fatigue test as discussed in Section 1. The BO coating was prepared according to the DIN 50938 standard for black oxidation. The preparation process included cleaning the steel components with alkaline solutions followed by immersing the components in a boiling aqueous alkaline bath at (< 150 °C) for a certain time. The components were then rinsed to remove the residual of the oxidation solution and to coat the steel components with rust preventing oil [33]. In their study the BO layer was prepared using single-bath, double-bath, and extended single-bath to achieve different thickness of the BO layer. The mechanical properties for the double-bath BO layer were examined using Continues Stiffness Measurement (CSM) Nano-indentation. Although the thickness of the double-bath BO layer in their study was estimated to be around 2 µm, their study reported the modulus of elasticity (E) and hardness (H) at the depth range of 200-300 nm only and the result obtained was a single value without measuring the variation across the depth. The single measurement could not obtain the properties across the entire thickness as seen in Figures 13 and 14, showing the gradual increase of the BO hardness and modulus of elasticity. It can be seen that the BO layer has different E and H values at different depths. Table 2 shows the average values of H and E of the BO layer at different depths. This table also included the values of E and H for the double-bath BO layer reported in [33]. It can be seen that the mechanical properties for the double-bath BO layer at 200-300 nm depth are fairly close to those found from the BO layer on the investigated bearing for the first 400 nm. The E and H values within this range of depth are considerably lower than those for the bearing steel; however, at further depths, the properties of the BO layer increase significantly. This can also be seen in Figures 13(b) and (c) where the E and H values of the remaining thin layer of the damaged BO layer, after the wear-out during service, are very close to the high values of E and H of the bearing steel. Accordingly, the

entire depth of this layer is required, which is achieved in this study using higher loads in the Nano-indentation system Hysitron TI Premier. The measurement and analysis of the thickness and mechanical properties of the damaged and undamaged BO layers of the investigated bearing also provided evidence showing that the BO coating did not fully alleviate the effect of surface traction to prevent damage initiation. The removal of the soft BO layer from the raceway surface might have affected the damage initiation at surface and subsurface because of the loss of this layer and the low mechanical properties of the near surface part of the BO layer. Therefore the remaining thin layer of the BO coating could not provide protection against the high friction force to prevent surface and subsurface damage initiation. It was difficult to determine how long this protective layer lasted but according to previous study [33], the BO layer could be worn off quickly under high slipping ratio conditions.

a)

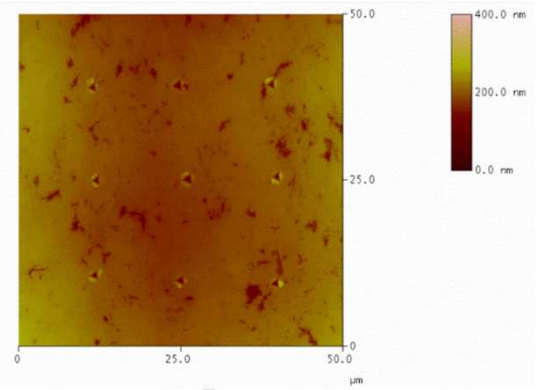

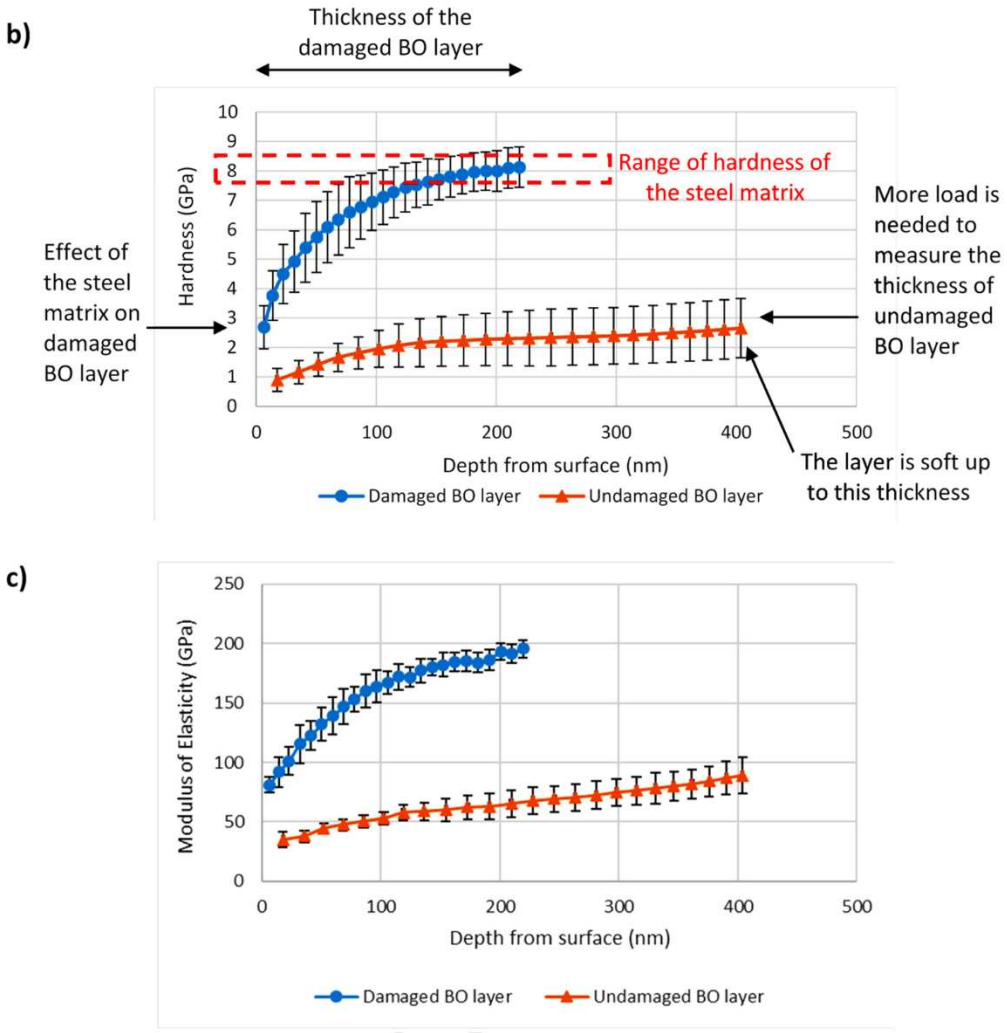

Figure 13: Damaged and undamaged BO layers: (a) AFM image showing Nano-indentation pattern on the surface of a sample from Region 1 in Figure 1; (b) Nano-indentation hardness; (c) Modulus of elasticity; measured using Hysitron Triboscope (± one standard deviation).

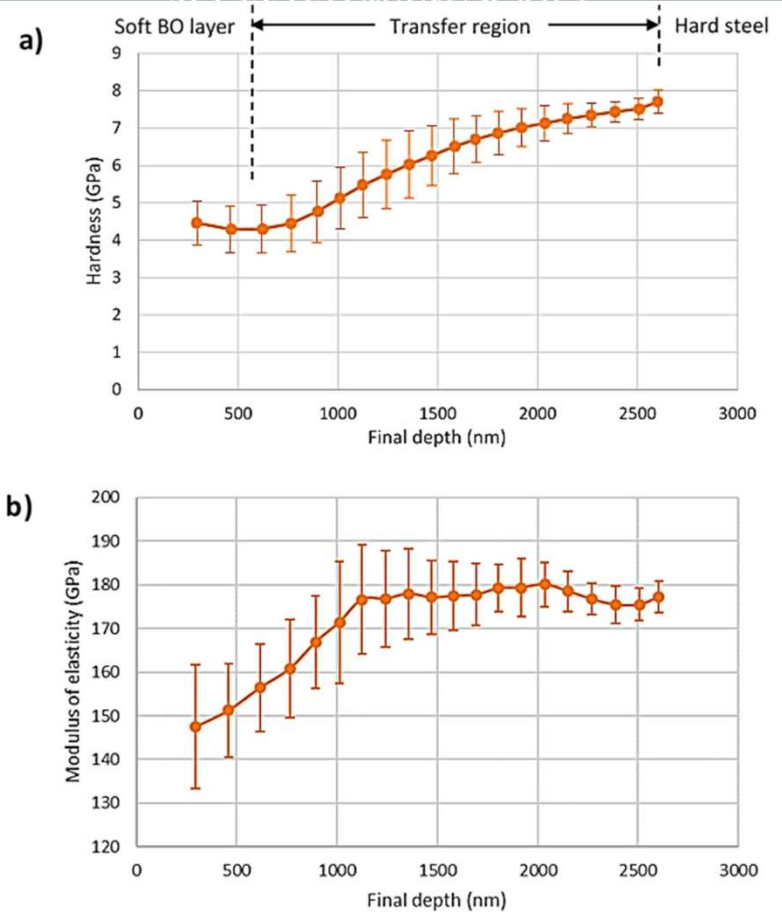

Figure 14: Undamaged BO layer: (a) Nano-indentation hardness; (b) Modulus of elasticity; measured using Hysitron TI Premier (± one standard deviations).

Table 2: BO layer characteristics (± one standard deviations)

	Average hardness (GPa)	Depth Range (nm)	Average modulus of elasticity (GPa)	Depth Range (nm)
Evans et al. [33]	2.6	200–300	61	80–100
Current work Low load	2.08±0.57	1-404	63.22±15.51	1-404
Current work High load	4.35±0.1	264-562	152±4.5	264-562
Current work High load in greater depths	6.12±1.2	264-2253	172±9.95	264-2253

5. Conclusions

Various forms of microstructural damage, including butterfly wings, WECs, subsurface cracks, surface-breaking RCF cracks, were found in the examined BO coated bearing. The following conclusions may be drawn:

1. The similarity of the microstructural damage, found in the examined BO coated bearing in this study and in the uncoated bearings reported in previous studies [10][13][14][38], showed that the BO coating was ineffective in preventing the subsurface microstructural damage of micro cracks and butterfly cracks initiated by non-metallic inclusions.
2. The non-metallic inclusions in the BO coated bearing were the main initiators of the subsurface damage in the form of butterfly wings. Inclusions of Types A, D and compound types initiated most of the subsurface damage. The total length of the butterfly wings or micro-cracks in the axially sectioned samples was found to be directly proportional to the inclusion size, resulted in greater microstructural damage due to longer inclusions.
3. The observed surface-breaking RCF cracks showed similarity to that of the subsurface WECs, especially when located far from the surface, with damage features indicting the effect of high surface traction. The surface examination showed different stages of spall formation on the raceway surface, which provided the evidence showing that the BO coating layer had not eliminated the damage caused by surface traction.
4. The variations of hardness and the modulus of elasticity across the thickness of the damaged and undamaged BO coating layers were measured. The thickness of the undamaged BO layer was around 2.2 μm while the damaged BO layer only had about 0.2 μm thickness remained. The hardness and modulus of elasticity of the damaged BO layer were very close to the high values of the bearing steel, significantly higher than that of the undamaged BO layer. For the first 400 nm of the undamaged BO layer the hardness and modulus of elasticity were considerably lower than those for the steel; however, at further depths of the BO layer, these properties increased significantly to reach the levels of the steel.
5. Surface and subsurface damage characterisations were conducted to the loaded zone as well as at the entrance and exit regions to the loaded zone of the raceway surface of the BO coated bearing. Subsurface micro cracks, butterfly cracks and WECs were extensively observed at the entrance region to the loaded zone of the bearing raceway surface where the BO coating layer was still partially intact. This provided evidences showing that the BO coating did not alleviate the effect of surface traction to prevent subsurface damage initiation. It further showed that there were multiple initiators leading to the WEA/WEC microstructural damage, such as non-metallic inclusions, in addition to the effect of surface traction and hydrogen absorption that the BO

Acknowledgments

The authors would like to acknowledge the support of Vestas Wind Systems A/S for sponsoring this research. The first author would like to thank the Iraqi Ministry of Higher Education and Scientific Research and the University of Baghdad for sponsoring his PhD study at the University of Sheffield.

References

[1] M. N. Kotzalas and G. L. Doll, "Tribological advancements for reliable wind turbine performance.," *Philos. Trans. A. Math. Phys. Eng. Sci.*, vol. 368, no. 1929, pp. 4829–4850, 2010.

[2] M. H. Evans, "An updated review: white etching cracks (WECs) and axial cracks in wind turbine gearbox bearings," *Mater. Sci. Technol. (United Kingdom)*, vol. 32, no. 11, pp. 1133–1169, 2016.

[3] M.-H. Evans, "White structure flaking (WSF) in wind turbine gearbox bearings: effects of 'butterflies' and white etching cracks (WECs)," *Mater. Sci. Technol.*, vol. 28, no. 1, pp. 3–22, Jan. 2012.

[4] A. M. Diederichs, A. Schwedt, J. Mayer, and T. Dreifert, "Electron microscopy analysis of structural changes within white etching areas," *Mater. Sci. Technol.*, no. 32:16, pp. 1683–1693, 2016.

[5] B. Gould and A. Greco, "The Influence of Sliding and Contact Severity on the Generation of White Etching Cracks," *Tribol. Lett.*, vol. 60:29, no. 2, pp. 1–13, 2015.

[6] J. Gegner and W. Nierlich, "The Bearing Axial Cracks Root Cause Hypothesis of Frictional Surface Crack Initiation and Corrosion Fatigue-Driven Crack Growth," in *NREL Wind Turbine Tribology Seminar*, 2011.

[7] B. Gould and A. Greco, "Investigating the Process of White Etching Crack Initiation in Bearing Steel," *Tribol. Lett.*, vol. 62:26, no. 2, pp. 1–14, 2016.

[8] J. Gegner and W. Nierlich, "Tribology Seminar Wind Turbine A Recap Tribology Seminar," in *NREL Wind Turbine Tribology Seminar*, 2011.

[9] M. Brückner, J. Gegner, A. Grabulov, W. Nierlich, and J. Slycke, "Butterfly formation mechanisms in rolling contact fatigue," in *Proc VHCF-5*, 2011, pp. 101–106.

[10] M. H. Evans, A. D. Richardson, L. Wang, and R. J. K. Wood, "Serial sectioning investigation of butterfly and white etching crack (WEC) formation in wind turbine gearbox bearings," *Wear*, vol. 302, no. 1–2, pp. 1573–1582, 2013.

[11] A. Grabulov, U. Ziese, and H. W. Zandbergen, "TEM/SEM investigation of microstructural changes within the white etching area under rolling contact fatigue and 3-D crack reconstruction by focused ion beam," *Scr. Mater.*, vol. 57, no. 7, pp. 635–638, 2007.

[12] V. Šmeļova, A. Schwedt, L. Wang, W. Holweger, and J. Mayer, "Microstructural changes in White Etching Cracks (WECs) and their relationship with those in Dark Etching Region (DER) and White Etching Bands (WEBs) due to Rolling Contact Fatigue (RCF)," *Int. J. Fatigue*, vol. 100, no. March, pp. 148–158, 2017.

[13] T. Bruce, E. Rounding, H. Long, and R. Dwyer-Joyce, "Characterisation of white etching crack damage in wind turbine gear- box bearings," *Wear*, vol. 338–339, pp. 164–177, 2015.

[14] H. A. Al-Tameemi, H. Long, and R. S. Dwyer-Joyce, "Initiation of sub-surface micro-cracks and

[16] M. H. Evans, A. D. Richardson, L. Wang, R. J. K. Wood, and W. B. Anderson, “Confirming subsurface initiation at non-metallic inclusions as one mechanism for white etching crack (WEC) formation,” *Tribol. Int.*, vol. 75, pp. 87–97, 2014.

[17] J.-H. Kang, R. H. Vegter, and P. E. J. Rivera-Díaz-del-Castillo, “Rolling contact fatigue in martensitic 100Cr6: Subsurface hardening and crack formation,” *Mater. Sci. Eng. A*, vol. 607, pp. 328–333, 2014.

[18] A. Warhadpande, F. Sadeghi, M. N. Kotzalas, and G. Doll, “Effects of plasticity on subsurface initiated spalling in rolling contact fatigue,” *Int. J. Fatigue*, vol. 36, no. 1, pp. 80–95, 2012.

[19] R. Errichello, R. Budny, and R. Eckert, “Investigations of Bearing Failures Associated with White Etching Areas (WEAs) in Wind Turbine Gearboxes,” *Tribol. Trans.*, vol. 56, no. 6, pp. 1069–1076, Nov. 2013.

[20] J. Gegner, “Tribological Aspects of Rolling Bearing Failures,” in *In: C.-H. Kuo (ed.), Tribology–Lubricants and Lubrication*, Rijeka, Croatia: InTech, 2011, pp. 33–94.

[21] T. Bruce, H. Long, and R. S. Dwyer-Joyce, “Dynamic modelling of wind turbine gearbox bearing loading during transient events,” *IET Renew. Power Gener.*, vol. 9, no. 7, pp. 821–830, 2015.

[22] H. Al-Hamadani, T. An, M. King, and H. Long, “System dynamic modelling of three different wind turbine gearbox designs under transient loading conditions,” *Int. J. Precis. Eng. Manuf.*, vol. 18, no. 11, pp. 1659–1668, 2017.

[23] N. T. Garabedian *et al.*, “The Cause of Premature Wind Turbine Bearing Failures : Overloading or Underloading ?,” *Tribol. Trans.*, vol. 0, no. 0, pp. 1–10, 2018.

[24] A. D. R. M. H. Evans, L. W. R. J. K. Wood, and M. I. B. Meuth, “The Evolution of White Etching Cracks (WECs) in Rolling Contact Fatigue - Tested 100Cr6 Steel,” *Tribol. Lett.*, vol. 66, no. 1, pp. 1–23, 2018.

[25] Y. S. Kang, R. D. Evans, and G. L. Doll, “IJTC2010-41191,” in *JTC2010*, 2010, pp. 1–3.

[26] J. Keller and S. Lambert, “Gearbox Instrumentation for the Investigation of Bearing Axial Cracking,” *NREL - Gearbox Reliab. Collab.*, no. NREL/TP-5000-70639, 2018.

[27] T. B. H. Long and R. S. D. Joyce, “Threshold Maps for Inclusion-Initiated Micro-Cracks and White Etching Areas in Bearing Steel : The Role of Impact Loading and Surface Sliding,” *Tribol. Lett.*, vol. 0, no. 0, p. 0, 2018.

[28] H. K. D. H. Bhadeshia, “Steels for bearings,” *Prog. Mater. Sci.*, vol. 57, no. 2, pp. 268–435, 2012.

[29] K. Stadler and A. Stubenrauch, “Premature bearing failures in industrial gearboxes,” *Annu. Rev. Mater. Sci.*, vol. 9, no. 1, pp. 283–311, 2013.

[30] R. Wood, J. Basumatary, and M. Evans, “Energy-related tribo-corrosion research at the National Centre for Advanced Tribology at Southampton,” *ASTM STP*, pp. 169–202, 2013.

[31] A. Ruellan, F. Ville, X. Kleber, A. Arnaudon, and D. Girodin, “Understanding white etching cracks in rolling element bearings: The effect of hydrogen charging on the formation mechanisms,” *Proc. Inst. Mech. Eng. Part J J. Eng. Tribol.*, vol. 228, no. 11, pp. 1252–1265, 2014.

[32] B. Mahmoudi, G. L. Doll, C. H. Hager, and R. D. Evans, “Influence of a WC/a-C: H tribological coating on micropitting wear of bearing steel,” *Wear*, vol. 350–351, pp. 107–115, 2016.

[33] R. Evans, C. H. Hager, Y. S. Kang, and G. Doll, “Comparison of black oxide and tungsten carbide reinforced diamond-like carbon(wc/a-c:H) surface treatments for rolling element bearings,” *Tribol. Trans.*, vol. 58, no. 3, pp. 444–453, 2015.

[34] K. Stadler, B. Han, V. Brizmer, and R. Pasaribu, “Benefits of using black oxidized bearings in wind applications,” *Bearing-news.com*, 2017. [Online]. Available: http://www.bearing-

[36] J. C. Gregory, “Chemical conversion coatings of metals to resist scuffing and wear,” *Tribol. Int.*, vol. 11, no. 2, pp. 105–112, 1978.

[37] J. Luyckx, “White Etching Crack Failure Mode in Roller Bearings: From Observation via Analysis to Understanding and an Industrial Solution,” *Roll. Elem. Bear. STP 1542, Yoshimi R. Tak. William F. Mandler, Ed.*, vol. doi:10.152, no. ASTM International, pp. 1–25, 2012.

[38] J. H. Al-Bedhany and H. Long, “Microscopic investigation of subsurface initiated damage of wind turbine gearbox bearings,” in *J. Phys.: Conf. Ser. 1106 012029*, 2018, pp. 1–9.

[39] K. Hui *et al.*, “The mechanism of intragranular acicular ferrite nucleation induced by Mg-Al-O inclusions,” *Adv. Mater. Sci. Eng.*, vol. 2015: 3786, 2015.

[40] ISO-4967, “ISO 4967 nonmetallic inclusions — Micrographic method using standard diagrams,” 2013.

[41] ASTM-E45-13, “Standard Test Methods for Determining the Inclusion Content of Steel,” *Am. Soc. Test. Mater.*, pp. 1–19, 2013.

[42] G. Guillonneau, G. Kermouche, S. Bec, and J. L. Loubet, “Determination of mechanical properties by nanoindentation independently of indentation depth measurement,” *J. Mater. Res.*, vol. 27, no. 19, pp. 2551–2560, 2012.

[43] X. Li and B. Bhushan, “A review of nanoindentation continuous stiffness measurement technique and its applications,” *Mater. Charact.*, vol. 48, no. 1, pp. 11–36, 2002.